Escape probability of a photon emitted near the black hole horizon

Kota Ogasawara,[1,*] Takahisa Igata,[2,†] Tomohiro Harada,[2,‡] and Umpei Miyamoto[3,§]

[1]*Theoretical Astrophysics Group, Department of Physics, Kyoto University, Kyoto 606-8502, Japan*
[2]*Department of Physics, Rikkyo University, Tokyo 171-8501, Japan*
[3]*RECCS, Akita Prefectural University, Akita 015-0055, Japan*

(Received 3 October 2019; accepted 27 January 2020; published 13 February 2020)

We investigate the escape of photons from the vicinity of the horizon to infinity in the Kerr-Newman black hole spacetime. We assume that a light source is at rest in a locally nonrotating frame on the equatorial plane and photons are emitted isotropically. Then, we evaluate the escape probability of the emitted photons. The main result of this paper is the following. If the black hole is extremal with the nondimensional spin parameter $a_* > 1/2$, however close to the horizon the light source would be, the escape probability remains nonzero. The near-horizon limit value of the escape probability is a monotonically increasing function of a_* and takes a maximum $\sim 29.1\%$ at $a_* = 1$, i.e., for the extremal Kerr case. On the other hand, if the black hole is extremal with $0 \leq a_* \leq 1/2$ or if the black hole is subextremal, the near-horizon limit value is zero.

DOI: 10.1103/PhysRevD.101.044023

I. INTRODUCTION

Very recently, the Event Horizon Telescope collaboration has succeeded in the first observation of the black hole shadows of the core of the galaxy M87 [1]. Although it remains controversial whether the central object forming the shadow is a black hole or not (see, e.g., Ref. [2] for a review), at least we have observed a photon ring scale near the ultracompact object directly through electromagnetic waves. As the observation progresses further, we will be able to clarify various properties of the center in the future. The brightness around the shadow depends on how often photons can escape from the source to infinity (i.e., the escape probability). Therefore, the evaluation of the probability is an important issue closely related to shadow observation.

The escape probability is also crucial in high-energy physics. In high-energy astrophysics, energetic particles are produced through the Penrose process [3,4] in the ergoregion, which plays a fundamental role in high-energy phenomena of our Universe. On the other hand, in the context of dark matter searches of high-energy astroparticle physics, exotic particles are produced by arbitrarily high-energy collisions near the horizon through the Banados-Silk-West (BSW) process [5] (see also, e.g., Ref. [6] for a review). More recently, an energy extraction process in a head-on collision—a combined process of the BSW and the Penrose—has attracted attention because the upper limit of its energy efficiency is of order 10 [7]. Moreover, it was shown that arbitrarily high efficiencies are achieved in the horizon limit by allowing that at least either of the colliding particles is emitted outwardly in the vicinity of the horizon before the collision. This is called the super-Penrose process [8]. The observability of such high-energy or exotic particles depends considerably on the escape probability.

In general, the production rate of high-energy particles in the ergoregion increases as the generating point approaches the horizon, while the size of the escape cone and the escape probability of photons emitted from there decrease [9–11].

Since a black hole is a spacetime region where nothing can escape, we can expect that the probability becomes zero if the emission arbitrarily approaches the horizon. Therefore, it is most likely that the observation of such energetic particles coming from the vicinity of the horizon seems impossible. In a previous work, however, we showed that the photon escape probability has a nonzero limiting value when the emission point arbitrarily approaches the horizon of the extremal Kerr black hole [12]. We found it in the context of the observability of high-energy photons produced by the super-Penrose process. This result implies that distant observers can see high-energy photons emitted from the vicinity of a rapidly rotating black hole.

Nonzero escape probability of photons in the horizon limit further suggests observability of various phenomena near the horizon. Although clarifying the conditions for this phenomenon is of significance, we still have not fully understood them. The extremal limit of a black hole seems to be a key to this phenomenon, but so far it is unclear whether this is a sufficient condition.

*kota@tap.scphys.kyoto-u.ac.jp
†igata@rikkyo.ac.jp
‡harada@rikkyo.ac.jp
§umpei@akita-pu.ac.jp

The purpose of this paper is to clarify the conditions for the escape probability remaining nonzero value when an emission point arbitrarily approaches the horizon. To achieve this, we adopt the Kerr-Newman spacetime as the background. Since the metric includes an electric charge parameter, the extremal limit is a one-parameter family of the black hole spin under fixed mass scale. The spin dependence allows us to consider the contribution of the extremal black hole rotation to the nonzero escape probability. In addition, we assume that the source stays at rest in the locally nonrotating frame (LNRF) on the equatorial plane and emits photons isotropically. These assumptions are motivated by the fact that the center-of-mass frame in a collisional Penrose process coincides with the LNRF. Moreover, since the LNRF does not corotate locally with the spacetime by definition, we can remove the contribution of proper orbital rotational motion of a source to the escape probability.

This paper is organized as follows. In the following section, we introduce the LNRF and obtain the components of the 4-momentum of a photon in the Kerr-Newman spacetime. In Sec. III, we show the ranges of an impact parameter for a photon that can escape from the vicinity of the horizon to infinity. In Sec. IV, focusing on the emission from a light source at rest in the LNRF, we introduce emission angles. The parameter ranges obtained in the previous section lead to the solid emission angle in which a photon can escape to infinity. Assuming isotropic emission, we define the escape probability. In Sec. V, we evaluate the escape probability and confirm that it becomes zero as the emission point approaches the horizon in general. However, in the extremal Kerr-Newman black hole with spin larger than a specific value, we observe that the probability remains a finite value even in the horizon limit. Section VI is devoted to the conclusion and discussions. In this paper, we use units in which $c = 1$ and $G = 1$.

II. GENERAL GEODESIC MOTION AND LOCALLY NONROTATING FRAME IN THE KERR-NEWMAN SPACETIME

The Kerr-Newman metric in the Boyer-Lindquist coordinates is given by

$$g_{\mu\nu}\mathrm{d}x^\mu \mathrm{d}x^\nu = -\frac{\Sigma\Delta}{A}\mathrm{d}t^2 + \frac{\Sigma}{\Delta}\mathrm{d}r^2 + \Sigma \mathrm{d}\theta^2 + \frac{A}{\Sigma}\sin^2\theta\left(\mathrm{d}\varphi - \frac{a(r^2+a^2-\Delta)}{A}\mathrm{d}t\right)^2, \quad (1)$$

where

$$\Sigma \equiv r^2 + a^2\cos^2\theta, \qquad \Delta \equiv r^2 - 2Mr + a^2 + e^2,$$
$$A \equiv (r^2+a^2)^2 - a^2\Delta\sin^2\theta. \quad (2)$$

This metric is parametrized by three parameters, mass M, spin a, and charge e. The spin parameter a is related to the angular momentum J with respect to the rotational axis as $a = J/M$. Without loss of generality, we assume that $a \geq 0$. Throughout this paper, we only consider the parameter range of the black hole spacetime, $a^2 + e^2 \leq M^2$. Then the event horizon is located at the radius $r = r_{\mathrm{H}} \equiv M + \sqrt{M^2 - a^2 - e^2}$, where Δ vanishes. The spacetime is stationary and axisymmetric with corresponding two Killing vectors ξ^μ and ψ^μ, where $\xi^\mu\partial_\mu = \partial_t$ and $\psi^\mu\partial_\mu = \partial_\varphi$.

Let us consider null geodesic motion with 4-momentum k^μ in the Kerr-Newman black hole spacetime. By using the Hamilton-Jacobi method [13], the components of k^μ are given by

$$k^t = \frac{1}{\Sigma}\left[a(L - aE\sin^2\theta) + \frac{r^2+a^2}{\Delta}[(r^2+a^2)E - aL]\right], \quad (3)$$

$$k^r = \frac{\sigma_r}{\Sigma}\sqrt{R}, \quad (4)$$

$$k^\theta = \frac{\sigma_\theta}{\Sigma}\sqrt{\Theta}, \quad (5)$$

$$k^\varphi = \frac{1}{\Sigma}\left[\frac{L}{\sin^2\theta} - aE + \frac{a}{\Delta}[(r^2+a^2)E - aL]\right], \quad (6)$$

where σ_r, $\sigma_\theta = \pm$, and

$$R \equiv [(r^2+a^2)E - aL]^2 - \Delta[(L-aE)^2 + \mathcal{Q}], \quad (7)$$

$$\Theta \equiv \mathcal{Q} - \cos^2\theta\left[\frac{L^2}{\sin^2\theta} - a^2E^2\right]. \quad (8)$$

Here $E = -\xi^\mu k_\mu$, $L = \psi^\mu k_\mu$, and $\mathcal{Q}$ are the conserved energy, angular momentum, and Carter constant, respectively.

We introduce the LNRF [14] that is a tetrad basis associated with observers who corotate with the background spacetime. The basis one-forms are given by

$$e^{(0)} = \sqrt{\frac{\Sigma\Delta}{A}}\mathrm{d}t, \quad e^{(1)} = \sqrt{\frac{\Sigma}{\Delta}}\mathrm{d}r, \quad e^{(2)} = \sqrt{\Sigma}\mathrm{d}\theta,$$
$$e^{(3)} = \sqrt{\frac{A}{\Sigma}}\sin\theta\mathrm{d}\varphi - \frac{a(r^2+a^2-\Delta)\sin\theta}{\sqrt{\Sigma A}}\mathrm{d}t. \quad (9)$$

These satisfy $g_{\mu\nu} = \eta_{(a)(b)}e^{(a)}_\mu e^{(b)}_\nu$, where $\eta_{(a)(b)} = \mathrm{diag}(-1,1,1,1)$, and a and b run from 0 to 3. The tetrad components of the 4-momentum, $k^{(a)} = e^{(a)}_\mu k^\mu$, are given by

$$k^{(0)} = \sqrt{\frac{\Delta}{\Sigma A}}\left[a(L - aE\sin^2\theta) + \frac{r^2+a^2}{\Delta}[(r^2+a^2)E - aL]\right], \quad (10)$$

$$k^{(1)} = \sigma_r\sqrt{\frac{R}{\Sigma\Delta}}, \quad (11)$$

$$k^{(2)} = \sigma_\theta \sqrt{\frac{\Theta}{\Sigma}}, \tag{12}$$

$$k^{(3)} = \frac{L}{\sin\theta}\sqrt{\frac{\Sigma}{A}}. \tag{13}$$

III. ESCAPE OF A PHOTON TO INFINITY

We consider the emission of a photon from the equatorial plane near the horizon $(r,\theta) = (r_*, \pi/2)$ to infinity. We adopt units in which $M = 1$ and assume that $a \neq 0$ in what follows.

We derive the conditions for a photon escaping to infinity. These are determined by investigating a radial turning point, i.e., $R = 0$. Introducing the dimensionless parameters

$$b \equiv \frac{L}{E}, \qquad q \equiv \frac{\mathcal{Q}}{E^2}, \tag{14}$$

for $E > 0$ and solving $R = 0$ for b, we obtain

$$b = b_1(r) \equiv \frac{a(e^2 - 2r) + \sqrt{\Delta[r^4 - q(\Delta - a^2)]}}{\Delta - a^2}, \tag{15}$$

and

$$b = b_2(r) \equiv \frac{a(e^2 - 2r) - \sqrt{\Delta[r^4 - q(\Delta - a^2)]}}{\Delta - a^2}. \tag{16}$$

We note that q is non-negative (i.e., $q \geq 0$) because Θ must be non-negative and $\Theta = \mathcal{Q}$ at the emission point $(r,\theta) = (r_*, \pi/2)$. The allowed parameter region of b for photon motion is given by

$$b \leq b_1 \quad \text{for } r_{\rm H} \leq r < 1 + \sqrt{1 - e^2}, \tag{17}$$

$$b_2 \leq b \leq b_1 \quad \text{for } 1 + \sqrt{1 - e^2} \leq r, \tag{18}$$

where b_2 diverges at $r = 1 + \sqrt{1 - e^2}$. We note that $b_2 \leq b$ for $r_{\rm H} \leq r < 1 + \sqrt{1 - e^2}$ is also the allowed region, but for a negative energy photon. Because such a photon cannot escape to infinity, we will not consider this region.

Now we focus on extremum points of b_i $(i = 1, 2)$. The positions are determined by the equation

$$b_i'(r) = 0. \tag{19}$$

Solving these for q, we obtain the single equation

$$q = f(r) \equiv \frac{r^2}{a^2}\left[-\frac{4(1-a^2-e^2)(r-e^2)}{(r-1)^2} + 3 - 4e^2 - (r-1)(r-3)\right]. \tag{20}$$

Note that the first term of f vanishes in the extremal case $a^2 + e^2 = 1$. Outside the horizon, $f(r)$ has the unique local maximum with the value f_0 at $r = r_0$, where

$$r_0(e) \equiv \frac{3 + \sqrt{9 - 8e^2}}{2}, \tag{21}$$

$$f_0(e) \equiv f(r = r_0) = \frac{r_0^4}{r_0 - e^2}. \tag{22}$$

It is worth noting that r_0 and f_0 depend only on e and monotonically decrease with respect to e in the range

$$r_0(1) = 2 \leq r_0 \leq 3 = r_0(0), \tag{23}$$

$$f_0(1) = 16 \leq f_0 \leq 27 = f_0(0), \tag{24}$$

and q satisfies the inequality

$$0 \leq q \leq f_0(e). \tag{25}$$

At the horizon, f takes the value

$$f(r_{\rm H}) = 4 - \frac{1}{a^2} \quad \text{for } a^2 + e^2 = 1, \tag{26a}$$

$$f(r_{\rm H}) = -\frac{r_{\rm H}^4}{a^2} \quad \text{for } a^2 + e^2 < 1. \tag{26b}$$

This implies that $f(r_{\rm H}) > 0$ only holds for $a^2 + e^2 = 1$ and $a > 1/2$. Then, we define two classes according to the sign of $f(r_{\rm H})$ as follows:

$$\text{Class I: } a^2 + e^2 = 1 \quad \text{and} \quad a > \frac{1}{2}, \tag{27a}$$

$$\text{Class II: } \begin{cases} a^2 + e^2 = 1 \quad \text{and} \quad a \leq \frac{1}{2} \\ \text{or} \\ a^2 + e^2 < 1. \end{cases} \tag{27b}$$

Under this classification, we consider the appearance of the roots of Eq. (20) outside the horizon, i.e., the radii of spherical photon orbits. For class I, Eq. (20) in the range $f(r_{\rm H}) < q \leq f_0$ has two roots $r_i(q)$ $(r_1 \leq r_2)$ outside the horizon. On the other hand, the equation in the range $0 \leq q \leq f(r_{\rm H})$ only has the largest root $r_2(q)$ outside the horizon, while has the next largest root $r_1(q)$ inside the horizon. For class II, Eq. (20) in the range $0 \leq q \leq f_0$ has the two roots $r_i(q)$ $(r_1 \leq r_2)$ outside the horizon. In both classes, r_i $(i = 1, 2)$ coincide with r_0 in the case $q = f_0$. In particular, if $q = 0$, the radii r_i reduce to those of circular photon orbits

$$r_{{\rm c},i} \equiv r_i(0). \tag{28}$$

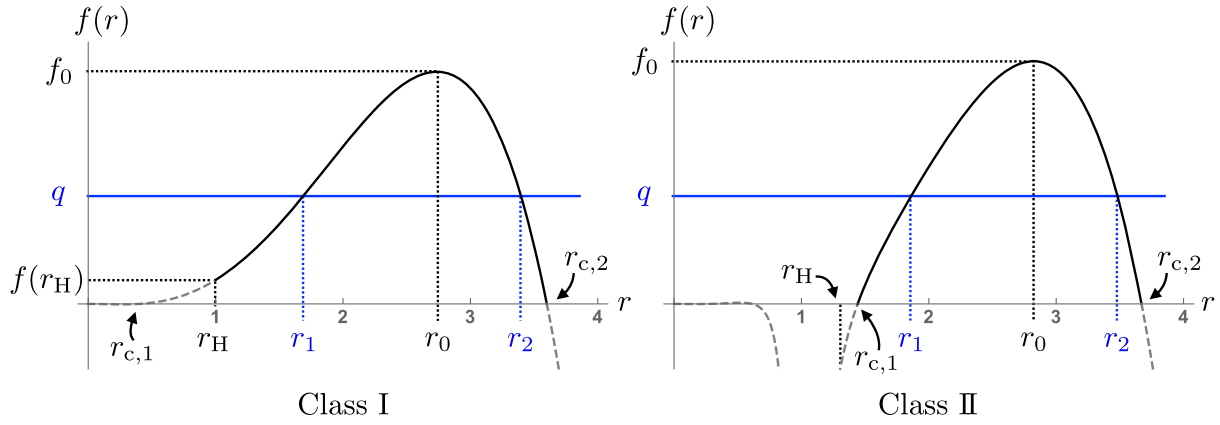

FIG. 1. Typical numerical plots of $f(r)$ (black solid and gray dashed lines). The black solid lines show $f(r)$ in the range $r > r_{\rm H}$ and $0 \le f \le f_0$. The intersections of the blue solid lines q and the black solid lines f give r_1 and r_2. We note that r_1 (r_2) is monotonically increasing (decreasing) with respect to q.

Therefore, in other words, the criterion of the classification in Eq. (26) is whether or not the radius of the innermost spherical photon orbit reaches the horizon. Figure 1 shows typical plots of $f(r)$ and the relations among $r_{\rm H}$, r_i, $r_{{\rm c},i}$, and r_0.

The extremum values of b_i become

$$b_i^{\rm s} \equiv b_i(r_i)|_{q=f(r_i)} = \frac{2(1-a^2-e^2)}{a(r_i-1)} - \frac{(r_i-1)^2}{a} + \frac{3-a^2-2e^2}{a}, \quad (29)$$

which are values of the impact parameter of photons on spherical photon orbits.

Let us consider the behavior of $b_i(r)$ to determine the range of b in which a photon can escape from $r = r_*$ to infinity. From now on, we consider the case where r_* is in the range $r_{\rm H} < r_* \le r_0$. We define three cases according to the relative position of r_1 to $r_{\rm H}$ and r_*:

$$\text{Case (a)} : r_1 < r_{\rm H} < r_*, \quad (30a)$$

$$\text{Case (b)} : r_{\rm H} \le r_1 < r_*, \quad (30b)$$

$$\text{Case (c)} : r_{\rm H} < r_* \le r_1, \quad (30c)$$

where case (a) appears only for class I.

For case (a), as r increases from $r_{\rm H}$ to ∞, b_1 begins with $b_1(r_{\rm H})$, where

$$b_1(r_{\rm H}) = a + \frac{1}{a} \quad (a^2+e^2=1), \quad (31a)$$

$$b_1(r_{\rm H}) = \frac{2(1+\sqrt{1-a^2-e^2})-e^2}{a} \quad (a^2+e^2<1), \quad (31b)$$

and monotonically increases to ∞. For cases (b) and (c), as r increases from $r_{\rm H}$ to ∞, b_1 begins with $b_1(r_{\rm H})$, monotonically decreases to a local minimum $b_1^{\rm s}$ at $r = r_1$, and monotonically increases to ∞. For all cases, as r increases from $r_{\rm H}$ to $1+\sqrt{1-e^2}$, b_2 begins with $b_2(r_{\rm H}) = b_1(r_{\rm H})$ and monotonically increases to ∞. As r increases from $1+\sqrt{1-e^2}$ to ∞, b_2 begins with $-\infty$, monotonically increases to a local maximum $b_2^{\rm s}$ at $r = r_2$, and monotonically decreases to $-\infty$. Figure 2 shows the schematic pictures of $b_i(r)$.

Then, the range of b in which a photon can escape to infinity is given as follows. In case (a), which appears only for class I, if photons are emitted radially inward (i.e., $\sigma_r = -$), then only those with $b_1(r_{\rm H}) < b < b_1(r_*)$ can escape to infinity [see the band between the green dashed lines in Fig. 2(a)]. If photons are emitted radially outward (i.e., $\sigma_r = +$), then only those with $b_2^{\rm s} < b \le b_1(r_*)$ can escape to infinity [see the band between the red dotted lines in Fig. 2(a)]. In case (b), which appears for both classes, if photons are emitted radially inward, then only those with $b_1^{\rm s} < b < b_1(r_*)$ can escape to infinity [see the band between the green dashed lines in Fig. 2(b)]. If photons are emitted radially outward, then only those with $b_2^{\rm s} < b \le b_1(r_*)$ can escape to infinity [see the band between the red dotted lines in Fig. 2(b)]. In case (c), which appears for both classes, if photons are emitted radially inward, then nothing can escape to infinity. If photons are emitted radially outward, then only those with $b_2^{\rm s} < b < b_1^{\rm s}$ can escape to infinity [see the band between the red dotted lines in Fig. 2(c)]. They are summarized in Table I.

IV. ESCAPE CONE AND CRITICAL ANGLES

We introduce the photon emission angles (α, β) from a light source at rest with respect to the LNRF

$$k^{(a)}|_{\substack{r=r_*\\ \theta=\pi/2}} \propto (1, \cos\alpha\sin\beta, -\cos\beta, \sin\alpha\sin\beta) \quad (-\pi \le \alpha < \pi \quad \text{and} \quad 0 \le \beta \le \pi), \quad (32)$$

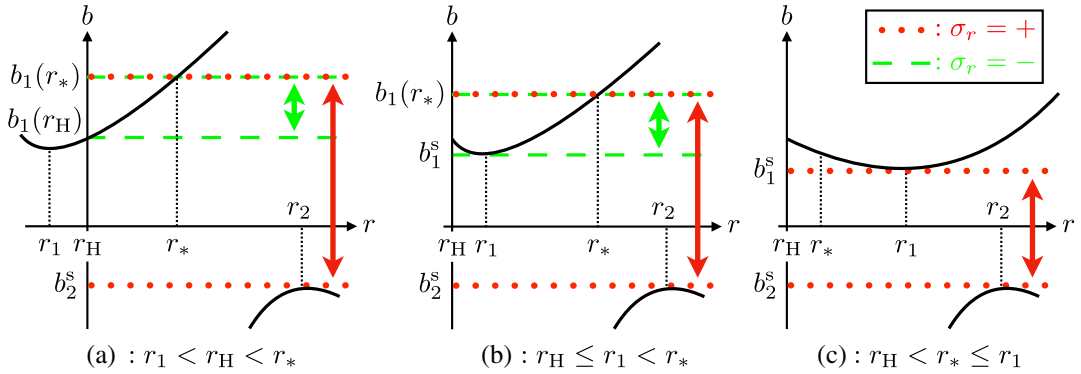

FIG. 2. Schematic pictures of $b_i(r)$ in cases (a)–(c). Upper and lower black solid lines denote $b_1(r)$ and $b_2(r)$, respectively. The range of b in which a photon can escape from $r = r_*$ to infinity depends on two conditions. One is whether a photon is emitted initially radially outward ($\sigma_r = +$) or inward ($\sigma_r = -$), and the other is the relative position of r_1 to r_H and r_*. If photons are emitted radially outward, the maximum and minimum values of b are given by the red dotted lines. If photons are emitted radially inward, the maximum and minimum values of b are given by the green dashed lines. We note that $b_2(r)$ in the range $r < 1 + \sqrt{1 - e^2}$ is not plotted.

TABLE I. Range of b in which a photon can escape from $(r, \theta) = (r_*, \pi/2)$ to infinity. The last column shows two pairs (σ_r, b) of the marginal parameter values with which a photon cannot escape to infinity for each cases.

Cases	q	$\sigma_r = +$	$\sigma_r = -$	Marginal pairs of (σ_r, b)
(a): $r_1 < r_H < r_*$	$0 \le q < f(r_H)$ (Class I)	$b_2^s < b \le b_1(r_*)$	$b_1(r_H) < b < b_1(r_*)$	$(+, b_2^s)$ and $(-, b_1(r_H))$
(b): $r_H \le r_1 < r_*$	$f(r_H) \le q < f(r_*)$ (Class I) $0 \le q < f(r_*)$ (Class II)	$b_2^s < b \le b_1(r_*)$	$b_1^s < b < b_1(r_*)$	$(+, b_2^s)$ and $(-, b_1^s)$
(c): $r_H < r_* \le r_1$	$f(r_*) \le q \le f_0$ (Classes I & II)	$b_2^s < b < b_1^s$	n/a	$(+, b_2^s)$ and $(+, b_1^s)$

or equivalently,

$$\sin\alpha \equiv \left.\frac{k^{(3)}}{\sqrt{(k^{(1)})^2 + (k^{(3)})^2}}\right|_{\substack{r=r_* \\ \theta=\pi/2}} = \left.\frac{br^2\sqrt{\Delta}}{\sqrt{A\hat{R} + b^2 r^4 \Delta}}\right|_{r=r_*}, \tag{33}$$

$$\cos\alpha \equiv \left.\frac{k^{(1)}}{\sqrt{(k^{(1)})^2 + (k^{(3)})^2}}\right|_{\substack{r=r_* \\ \theta=\pi/2}} = \left.\frac{\sigma_r\sqrt{A\hat{R}}}{\sqrt{A\hat{R} + b^2 r^4 \Delta}}\right|_{r=r_*}, \tag{34}$$

$$\sin\beta \equiv \left.\frac{\sqrt{(k^{(1)})^2 + (k^{(3)})^2}}{\sqrt{(k^{(1)})^2 + (k^{(2)})^2 + (k^{(3)})^2}}\right|_{\substack{r=r_* \\ \theta=\pi/2}} = \left.\frac{\sqrt{A\hat{R} + b^2 r^4 \Delta}}{a(b-a)\Delta + (r^2 + a^2)(r^2 - ab + a^2)}\right|_{r=r_*}, \tag{35}$$

$$\cos\beta \equiv \left.\frac{-k^{(2)}}{\sqrt{(k^{(1)})^2 + (k^{(2)})^2 + (k^{(3)})^2}}\right|_{\substack{r=r_* \\ \theta=\pi/2}} = -\left.\frac{\sigma_\theta\sqrt{q\Delta A}}{a(b-a)\Delta + (r^2 + a^2)(r^2 - ab + a^2)}\right|_{r=r_*}, \tag{36}$$

where $\hat{R} = R/E^2$. Thus α is the angle between $e^{(1)}$ and k projected onto the equatorial plane, which is positive in the direction $e^{(3)}$, and β is the angle between $-e^{(2)}$ and k, where k is the projection of k^μ normal to $e^{(0)}$. We illustrate the relation between the LNRF and (α, β) in Fig. 3. The definition of α, β means that the angles are functions of σ_r, σ_θ, b, q, and r_* as

$$\alpha(\sigma_r, b, q, r_*), \qquad \beta(\sigma_\theta, b, q, r_*). \tag{37}$$

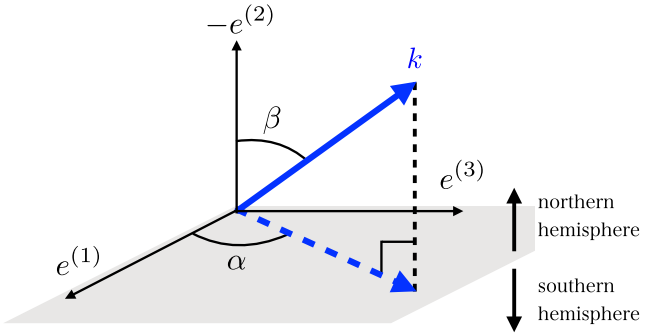

FIG. 3. Emission angles (α, β) defined in the LNRF where the origin coincides with the emission point $(r, \theta) = (r_*, \pi/2)$. Here k is the projection of k^μ normal to $e^{(0)}$. In this figure, upward and downward directions represent northward and southward directions of the Kerr-Newman black hole, respectively.

The range of α is restricted depending on the sign of b and σ_r as follows. If photons are emitted radially inward (i.e., $\sigma_r = -$), we have

$$-\pi \le \alpha \le -\frac{\pi}{2} \quad \text{for } b \le 0, \tag{38}$$

$$\frac{\pi}{2} \le \alpha < \pi \quad \text{for } b > 0, \tag{39}$$

where $\alpha = -\pi$ holds for $b = 0$. If photons are emitted radially outward (i.e., $\sigma_r = +$), we have

$$-\frac{\pi}{2} \le \alpha \le 0 \quad \text{for } b \le 0, \tag{40}$$

$$0 \le \alpha \le \frac{\pi}{2} \quad \text{for } b \ge 0, \tag{41}$$

where $\alpha = 0$ holds for $b = 0$. The range of β depends on σ_θ as

$$0 \le \beta \le \frac{\pi}{2} \quad \text{for } \sigma_\theta = -, \tag{42}$$

$$\frac{\pi}{2} \le \beta \le \pi \quad \text{for } \sigma_\theta = +. \tag{43}$$

Note that when $q = 0$, k is confined in the equatorial plane (i.e., $\beta = \pi/2$).

In terms of α and β, we define an escape cone S to be the solid angle of emission that allows photons to escape to infinity. Assuming that photons are emitted isotropically, we can define the escape probability $P(r_*)$ by

$$P(r_*) \equiv \frac{1}{4\pi} \int_S \mathrm{d}\alpha \mathrm{d}\beta \sin\beta. \tag{44}$$

Since the Kerr-Newman spacetime is symmetric to the equatorial plane, the escape probability of isotropic emission to the northern hemisphere is the same with that to the southern hemisphere. Therefore we only need to consider the emission to the northern hemisphere (i.e., $\sigma_\theta = -$). To evaluate P, we determine the critical angles, which are points on the boundary of S. There is a one-to-one correspondence between the critical angles and the parameter set (σ_r, b, q) of photons that cannot marginally escape to infinity.

Let us specify such parameter sets for each case. In case (a), if photons with $b = b_1(r_{\rm H})$ are emitted radially inward (i.e., $\sigma_r = -$), then they arbitrarily approach the horizon but cannot escape to infinity [see Fig. 2(a)]. If photons with $b = b_2^{\rm s}$ are emitted radially outward (i.e., $\sigma_r = +$), then they arbitrarily approach $r = r_2$ but cannot escape to infinity. In case (b), if photons with $b = b_1^{\rm s}$ are emitted radially inward, then they arbitrarily approach $r = r_1$ [see Fig. 2(b)]. If photons with $b = b_2^{\rm s}$ are emitted radially outward, then they arbitrarily approach $r = r_2$. In case (c), if photons with $b = b_i^{\rm s}$ are emitted radially outward, then they arbitrarily approach $r = r_i$ but cannot escape to infinity [see Fig. 2(c)].

We find that all the parameter pairs appear as the boundary of the ranges for photons that can escape to infinity [see Table I]. Therefore, we call them the marginal pairs. They are summarized in the last column of Table I. Finally we obtain the critical angles (α_i, β_i) $(i = 1, 2)$ relevant to marginal parameter values associated with b_i and their total set ∂S (i.e., the boundary of S) as follows:

$$\partial S = \bigcup_{i=1,2} \{(\alpha_i, \beta_i) | 0 \le q \le f_0\}, \tag{45}$$

where

$$(\alpha_1, \beta_1) \equiv (\alpha_{1(\rm a)}, \beta_{1(\rm a)}) \equiv (\alpha, \beta)|_{\substack{\sigma_r = - \\ b = b_1(r_{\rm H})}} \quad \text{for } 0 \le q < f(r_{\rm H}) \quad [\text{case (a)}], \tag{46a}$$

$$(\alpha_1, \beta_1) \equiv (\alpha_{1(\rm b)}, \beta_{1(\rm b)}) \equiv (\alpha, \beta)|_{\substack{\sigma_r = - \\ b = b_1^{\rm s}}} \quad \text{for } f(r_{\rm H}) \le q < f(r_*) \quad [\text{case (b)}], \tag{46b}$$

$$(\alpha_1, \beta_1) \equiv (\alpha_{1(\rm c)}, \beta_{1(\rm c)}) \equiv (\alpha, \beta)|_{\substack{\sigma_r = + \\ b = b_1^{\rm s}}} \quad \text{for } f(r_*) \le q \le f_0 \quad [\text{case (c)}], \tag{46c}$$

in class I,

$$(\alpha_1, \beta_1) \equiv (\alpha_{1(\rm b)}, \beta_{1(\rm b)}) \equiv (\alpha, \beta)|_{\substack{\sigma_r = - \\ b = b_1^{\rm s}}} \quad \text{for } 0 \le q < f(r_*) \quad [\text{case (b)}], \tag{47a}$$

$$(\alpha_1, \beta_1) \equiv (\alpha_{1(\rm c)}, \beta_{1(\rm c)}) \equiv (\alpha, \beta)|_{\substack{\sigma_r = + \\ b = b_1^{\rm s}}} \quad \text{for } f(r_*) \le q \le f_0 \quad [\text{case (c)}], \tag{47b}$$

in class II, and

$$(\alpha_2, \beta_2) \equiv (\alpha, \beta)|_{\substack{\sigma_r = + \\ b = b_2^{\rm s}}} \quad \text{for } 0 \le q \le f_0 \quad [\text{cases (a)–(c)}], \tag{48}$$

in classes I and II. Note that once we fix the value of r_*, then the critical angles (α_i, β_i) depend only on q, i.e., $\alpha_i = \alpha_i(q)$ and $\beta_i = \beta_i(q)$. Figure 4 shows a schematic picture of the critical angles.

V. ESCAPE PROBABILITY

In this section, we evaluate the escape probability P for a photon in Eq. (44). Let $\alpha_{\rm min}$ and $\alpha_{\rm max}$ be the minimum and the maximum of the critical angle, and $\beta_{\rm min}(\alpha)$ and $\beta_{\rm max}(\alpha)$ be the minimum and the maximum of the critical angle for a given α. Assuming that S is convex, we obtain

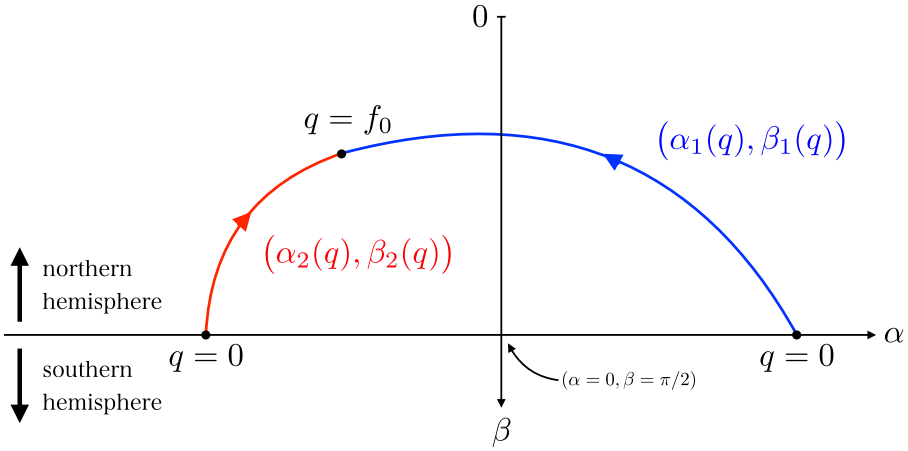

FIG. 4. Schematic picture of the critical angles with fixed r_* for the northern hemisphere in $\alpha - \beta$ plane. The blue and red solid lines show $(\alpha_1(q), \beta_1(q))$ and $(\alpha_2(q), \beta_2(q))$ for $0 \le q \le f_0$, respectively. We plot the critical angles as functions of q because we have chosen σ_r, σ_θ, and b for the critical angles. The critical angle $\alpha_1(q)$ $(\alpha_2(q))$ is monotonically decreasing (increasing) with respect to q. We note that the critical angles in the southern hemisphere is symmetrical about the α-axis.

$$P = \frac{1}{4\pi}\int_{\alpha_{\min}}^{\alpha_{\max}} d\alpha \int_{\beta_{\min}(\alpha)}^{\beta_{\max}(\alpha)} d\beta \sin\beta = \frac{1}{2\pi}\int_{\alpha_{\min}}^{\alpha_{\max}} d\alpha \cos\beta_{\min}(\alpha), \tag{49}$$

where we have used $\beta_{\max} = \pi - \beta_{\min}$. Using the critical angles (α_i, β_i) and the relation between q and r_i given in Eq. (20) [see also Figs. 1 and 4], we change the integration variable α of Eq. (49) to r_i as

$$P = P_1 + P_2, \tag{50}$$

where

$$P_i = \frac{(-1)^i}{2\pi}\int_0^{f_0} dq \frac{d\alpha_i}{dq}\cos\beta_i = \frac{(-1)^i}{2\pi}\int_{r_{c,i}}^{r_0} dr_i \frac{d\alpha_i}{dr_i}\cos\beta_i. \tag{51}$$

In particular, using the definition of the critical angles in Eqs. (46)–(48), we can reduce P_1 as

$$\begin{aligned} P_1 = &-\frac{1}{2\pi}\int_{r_{c,1}}^{r_H} dr_1 \frac{d\alpha_{1(a)}}{dr_1}\cos\beta_{1(a)} \\ &-\frac{1}{2\pi}\int_{r_H}^{r_*} dr_1 \frac{d\alpha_{1(b)}}{dr_1}\cos\beta_{1(b)} \\ &-\frac{1}{2\pi}\int_{r_*}^{r_0} dr_1 \frac{d\alpha_{1(c)}}{dr_1}\cos\beta_{1(c)} \quad \text{(class I)}, \end{aligned} \tag{52a}$$

$$\begin{aligned} P_1 = &-\frac{1}{2\pi}\int_{r_{c,1}}^{r_*} dr_1 \frac{d\alpha_{1(b)}}{dr_1}\cos\beta_{1(b)} \\ &-\frac{1}{2\pi}\int_{r_*}^{r_0} dr_1 \frac{d\alpha_{1(c)}}{dr_1}\cos\beta_{1(c)} \quad \text{(class II)}. \end{aligned} \tag{52b}$$

It is useful to note that some of the integrands in the above integrals have a common form

$$\begin{aligned} \frac{d\alpha_{1(b)}}{dr_1}\cos\beta_{1(b)}\bigg|_{r_1=x} &= \frac{d\alpha_{1(c)}}{dr_1}\cos\beta_{1(c)}\bigg|_{r_1=x} \\ &= \frac{d\alpha_2}{dr_2}\cos\beta_2\bigg|_{r_2=x} \equiv g(x). \end{aligned} \tag{53}$$

Finally, from Eqs. (49)–(53), P is given by

$$P = -\frac{1}{2\pi}\int_{r_{c,1}}^{r_H} dr_1 \frac{d\alpha_{1(a)}}{dr_1}\cos\beta_{1(a)} - \frac{1}{2\pi}\int_{r_H}^{r_{c,2}} dx g(x) \quad \text{(class I)}, \tag{54a}$$

$$P = -\frac{1}{2\pi}\int_{r_{c,1}}^{r_{c,2}} dx g(x) \quad \text{(class II)}. \tag{54b}$$

A. Extremal Kerr black hole

We evaluate the critical angles and escape probability in the extremal Kerr black hole. Since $a = 1$ and $e = 0$ (i.e., class I), the function $f(r)$ in Eq. (20) reduces to

$$f(r) = r^3(4 - r), \tag{55}$$

which has the maximum value $f_0 = 27$ at $r_0 = 3$ and zeros at the radii of circular photon orbits

$$r_{c,1} = 0, \qquad r_{c,2} = 4. \tag{56}$$

Furthermore, the values of b given in Eqs. (29) and (31a) are of the form

$$b_i^s = -r_i^2 + 2r_i + 1, \tag{57}$$

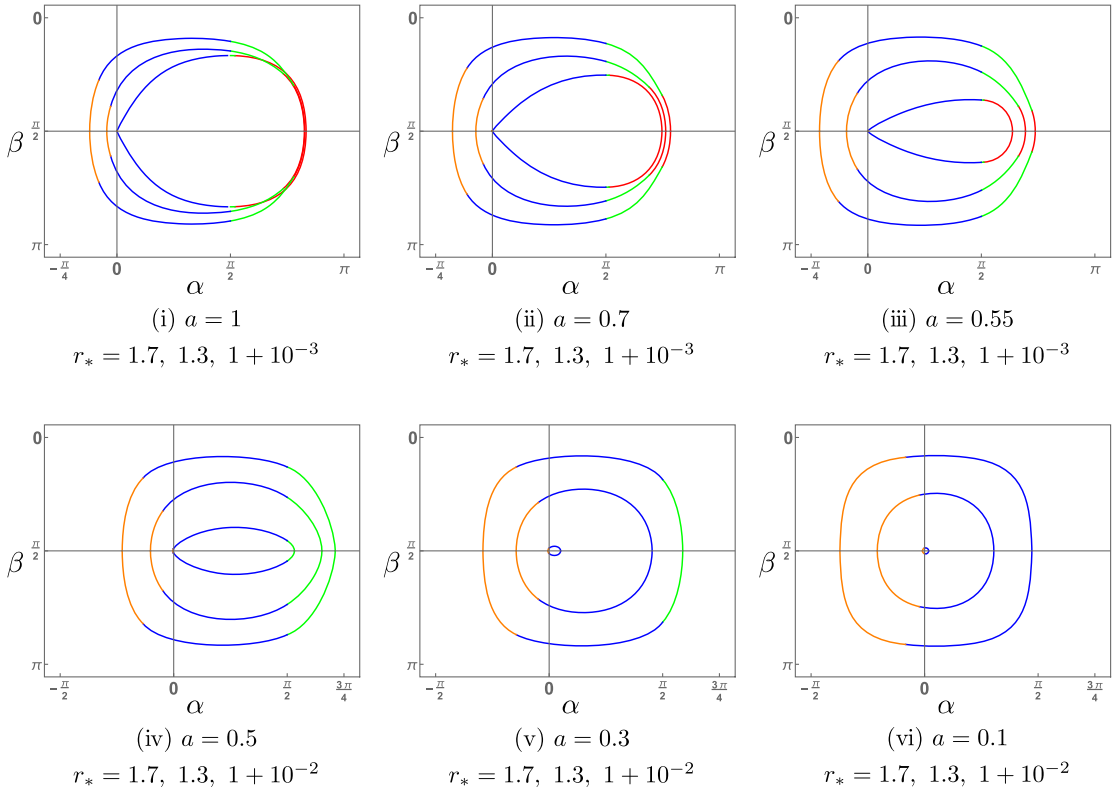

FIG. 5. Critical angles in $\alpha - \beta$ plane in the extremal Kerr-Newman black hole. The red, green, blue, and orange lines show $(\alpha_{1(a)}, \beta_{1(a)})$, $(\alpha_{1(b)}, \beta_{1(b)})$, $(\alpha_{1(c)}, \beta_{1(c)})$, and (α_2, β_2), respectively. We set $r_* = 1.7, 1.3, 1 + 10^{-3}$ for class I (the upper three panels) and $r_* = 1.7, 1.3, 1 + 10^{-2}$ for class II (the lower three panels) from outside to inside. The inside of each closed solid curve shows the escape cone S. We can see that, in the near-horizon emission case for class I, the presence of the critical angles in case (a) prevents the escape cone from disappearing.

$$b_1(r_{\rm H}) = 2, \tag{58}$$

where $r_{\rm H} = 1$.

Using these expressions, we can evaluate the critical angles (α_i, β_i). In Fig. 5, we find sets of critical angles ∂S for several values of r_*. As r_* decreases toward $r_{\rm H} = 1$, the size of the escape cone S decreases. However, we should notice that S still has enough size, even if r_* is close enough to the horizon [see $r_* = 1.001$ case]. Now let us evaluate the escape probability P in Eq. (54a) with the above expressions. In Fig. 6, the solid black line shows P as a function of r_*. We find that P decreases as r_* decreases toward $r_{\rm H}$ but is nonzero in the horizon limit. Indeed, the value of P in the horizon limit takes

$$\lim_{r_* \to 1} P = 0.2916\ldots. \tag{59}$$

This result means that about 30% of photons isotropically emitted from a light source near the horizon of the extremal Kerr black hole can escape to infinity.

Here let us confirm that the result of Ref. [12] can be reproduced. Assuming that photons are emitted isotropically but confined in the equatorial plane, we can identify the escape cone with the segment $\alpha \in [\alpha_2, \alpha_{1(a)}]|_{q=0}$ on the line $\beta = \pi/2$ in Fig. 5(i). Thus the escape probability in such a situation is given by

$$P = \frac{(\alpha_{1(a)} - \alpha_2)|_{q=0}}{2\pi}, \tag{60}$$

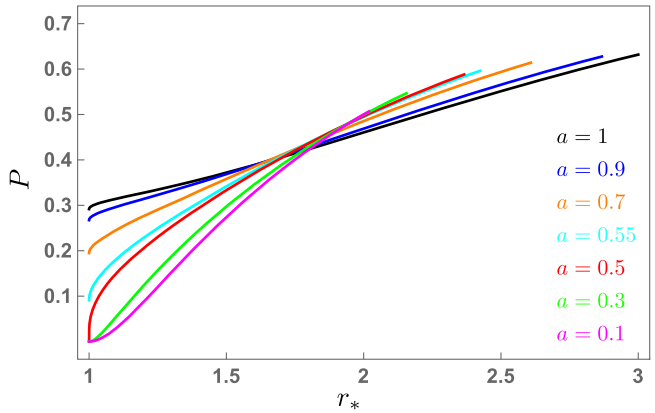

FIG. 6. Escape probability in the extremal Kerr-Newman black hole.

TABLE II. Escape probability evaluated at $r_* = 1 + \varepsilon$ in the extremal Kerr-Newman black hole.

	$a = 1$	$a = 0.9$	$a = 0.7$	$a = 0.55$	$a = 0.5$	$a = 0.3$	$a = 0.1$
$\varepsilon = 10^{-1}$	3.14×10^{-1}	2.96×10^{-1}	2.45×10^{-1}	1.81×10^{-1}	1.50×10^{-1}	5.52×10^{-2}	3.02×10^{-2}
$\varepsilon = 10^{-3}$	2.93×10^{-1}	2.69×10^{-1}	1.98×10^{-1}	9.92×10^{-2}	3.27×10^{-2}	1.62×10^{-5}	4.52×10^{-6}
$\varepsilon = 10^{-5}$	2.91×10^{-1}	2.67×10^{-1}	1.95×10^{-1}	9.19×10^{-2}	9.91×10^{-3}	1.64×10^{-9}	4.54×10^{-10}
$\varepsilon \to 0$	2.91×10^{-1}	2.67×10^{-1}	1.94×10^{-1}	9.11×10^{-2}	0	0	0

and the horizon limit of this expression is $5/12$. This is consistent with the result of Ref. [12].

B. Extremal Kerr-Newman black hole

We evaluate the critical angles and escape probability in the extremal Kerr-Newman black hole (i.e., $a^2 + e^2 = 1$). Therefore, we replace e in all the above expressions with $\sqrt{1 - a^2}$. Then, $f(r)$ reduces to

$$f(r) = -\frac{r^2}{a^2}(r - r_{c,1})(r - r_{c,2}), \tag{61}$$

where

$$r_{c,1} = 2(1 - a), \qquad r_{c,2} = 2(1 + a). \tag{62}$$

This function has the maximum with the value

$$f_0 = \frac{(\sqrt{1 + 8a^2} - 1)(\sqrt{1 + 8a^2} + 3)^3}{16a^2} \tag{63}$$

at $r = r_0 = (\sqrt{1 + 8a^2} + 3)/2$. Furthermore, the values of b given in Eqs. (29) and (31a) are of the form

$$b_i^{\mathrm{s}} = \frac{-r_i^2 + 2r_i + a^2}{a}, \qquad b_1(r_{\mathrm{H}}) = a + \frac{1}{a}, \tag{64}$$

where $r_{\mathrm{H}} = 1$.

The critical angles with the above expressions are shown in Fig. 5. We can confirm that even if r_* is close enough to r_{H}, the escape cones in class I have a nonzero size in the region $\alpha > 0$. On the other hand, as r_* approaches r_{H} sufficiently, the escape cones in class II shrink to the origin

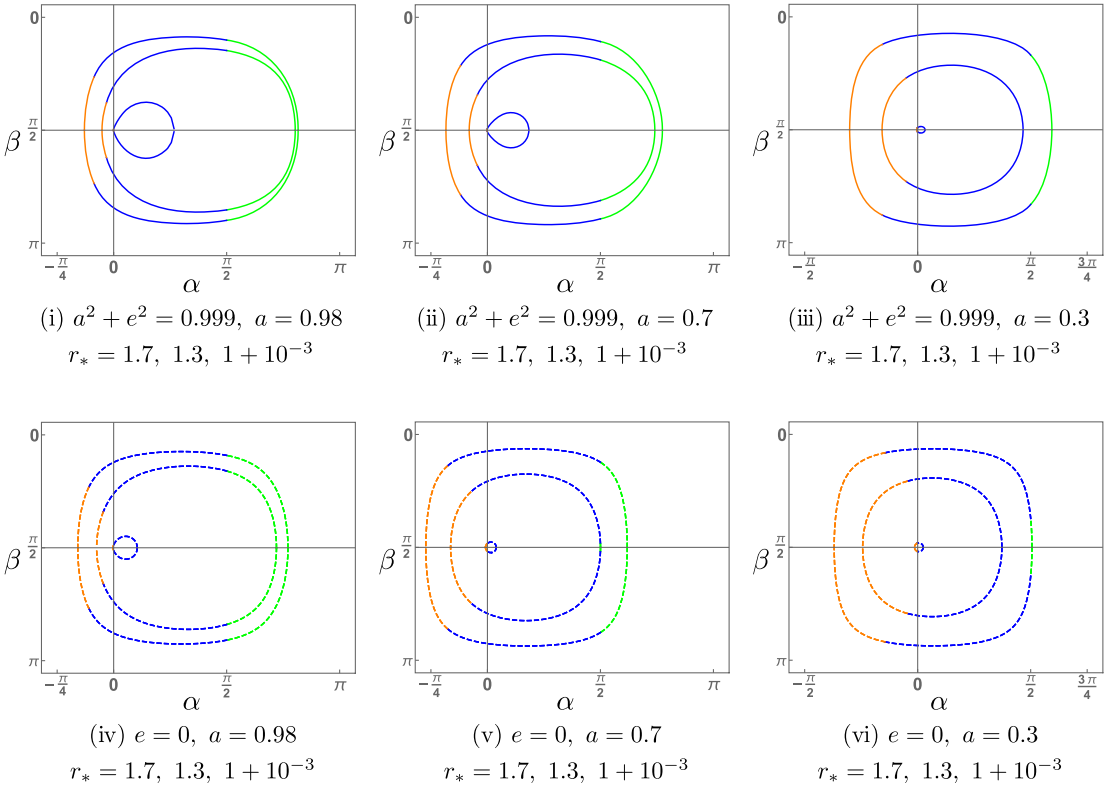

FIG. 7. Critical angles in $\alpha - \beta$ plane in nonextremal black holes. The green, blue, and orange lines show $(\alpha_{1(b)}, \beta_{1(b)})$, $(\alpha_{1(c)}, \beta_{1(c)})$, and (α_2, β_2), respectively. The solid lines (the upper three panels) and dashed lines (the lower three panels) are the cases of $a^2 + e^2 = 0.999$ and $e = 0$, respectively. For each panel, we set $r_* = 1.7,\ 1.3,\ 1 + 10^{-3}$ from outside to inside.

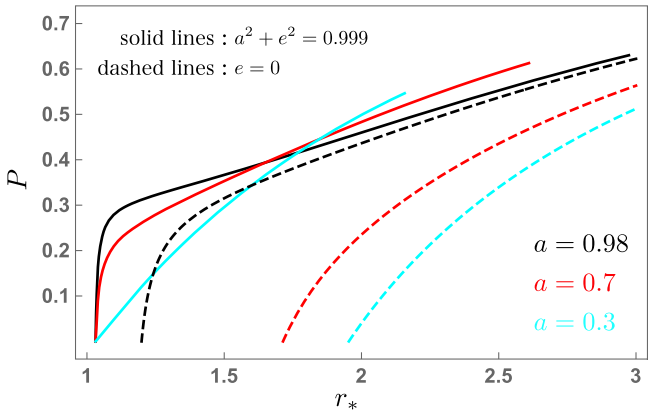

FIG. 8. Escape probability in nonextremal black holes. The solid and dashed lines are the cases of $a^2+e^2=0.999$ and $e=0$, respectively.

of the $\alpha-\beta$ plane. The critical angles $(\alpha_{1(a)},\beta_{1(a)})$ that appears only in class I seem to prevent the escape cones in the horizon limit from disappearing. This is consistent with the result of Refs. [9,10].

Figure 6 shows the numerical plots of the escape probability for various values of a.[1] As r_* decreases, P monotonically decreases in common regardless of a. On the other hand, qualitative difference depending on a appears in near-horizon emissions. In the horizon limit, P takes a nonzero value for class I while it vanishes for class II. Some explicit values of P for near-horizon emissions are shown in Table II. We should note that P in the horizon limit monotonically increases as a increases in class I. Hence, we find that the maximum value of P in the horizon limit is the case of the extremal Kerr black hole.

C. Nonextremal black holes

Finally, we show some examples of the critical angles and escape probability in nonextremal black holes, where $a^2+e^2=0.999$ with $a=0.98$, 0.7, 0.3 and $e=0$ with $a=0.98$, 0.7, 0.3. The critical angles and escape probability with the above cases are shown in Figs. 7 and 8, respectively. We find that both the sizes of S and P are monotonically decreasing as r_* decreases. In the horizon limit, S shrinks to the origin of the $\alpha-\beta$ plane and P becomes zero. However, in rapidly rotating and near-extremal cases, even if r_* is close to $r_{\rm H}$, the escape cones have a relatively large size [see Figs. 7(i) and 7(ii)]. Similarly, the escape probability takes a relatively large value up to the very vicinity of the horizon, and finally approaches zero rapidly.

[1]The integral of the first term in Eq. (54a) is evaluated analytically:

$$-\frac{1}{2\pi}\int_{r_{c,1}}^{r_{\rm H}} dr_1 \frac{d\alpha_{1(a)}}{dr_1}\cos\beta_{1(a)} = \frac{1}{2\pi}\left[\arctan\left(\frac{(1+a^2)r_*^2}{a[r_*-1+(r_*+1)(r_*^2+a^2)]}\sqrt{\frac{4-1/a^2}{(r_*-1)(r_*-3)}}\right) - \frac{(1+a^2)r_*^2}{a[r_*-1+(r_*+1)(r_*^2+a^2)]}\arctan\sqrt{\frac{4-1/a^2}{(r_*-1)(r_*-3)}}\right]. \quad (65)$$

The horizon limit of this expression is $1/4-1/(8a)$.

VI. CONCLUSION AND DISCUSSIONS

We have examined the escape of photons from the vicinity of the horizon to infinity in the Kerr-Newman black hole spacetime. We have evaluated escape cones at an emission point staying at rest in the LNRF and also the escape probability under assuming isotropic emission. Our main result is that when the black hole is extremal and has the spin parameter larger than $1/2$, even if the light source arbitrarily approaches the horizon, the escape cone does not shrink and the escape probability remains nonzero. Furthermore, the nonzero escape probability in the horizon limit monotonically increases as the spin increases from $1/2$ with remaining extremal. Consequently, in the extremal Kerr black hole, it takes the largest value, 0.2916…. However, we should kept in mind that this result may not apply to light sources that are not on the equatorial plane.

The reason for the nonvanishing photon escape probability in the horizon limit is that photons can be reflected at a radius arbitrarily close to the horizon. This phenomenon is also related to the fact that the radius of the innermost spherical photon orbit coincides with the horizon radius.

Even for extremal black holes, the escape probability in the horizon limit becomes zero if the spin parameter is equal to or less than $1/2$. Similarly, it does in the case of nonextremal black holes. However, in rapidly rotating and near-extremal black hole spacetime, as the emission point approaches the horizon, the escape probability keeps a relatively large nonzero value until it reaches a near-horizon region, and finally becomes zero when it reaches just outside the horizon. Even in this case, the fact that photons can be reflected at a radius very close to the horizon is essential [15].

Our result is that up to approximately 30% of photons emitted from the light source near the horizon of the rapidly rotating (near-)extremal black hole escape to infinity. Hence, the phenomenon near the horizon of such a rapidly rotating and (near-)extremal black hole (e.g., the Penrose process or the black hole shadow) must be relatively visible compared to the case of a slowly rotating black hole. We speculate the effect of the nonzero escape probability on black hole shadow observations. Photons arriving at the shadow edge have been scattered at the radii of spherical photon orbits in the past. In particular, for rapidly rotating black holes, photons reaching the innermost shadow edge have been scattered at almost the horizon radius. Therefore,

observing the innermost shadow edge is equivalent to observing a near-horizon region of the black hole. In fact, one of the estimates based on the observations of the M87 galactic center suggests that the central object may be rapidly rotating [16]. Therefore, according to our results, a sufficient number of photons scattered at almost the horizon radius reach the innermost edge of the shadow, so that we can observe a near-horizon region through them.

The photon emission from several sources in the Kerr spacetime was considered by Ref. [9] and off the equatorial plane in the Kerr–Newman spacetime was considered by Ref. [10]. The escape cones calculated in these previous works and the escape probability we showed have the same qualitative behavior in that they monotonically decrease as the photon emission point approaches the horizon. Although we might also infer that the escape probability off the equatorial plane might be smaller than that from the equatorial plane, more careful comparisons would be useful for further developments. It is also useful to calculate the escape probability off the equatorial plane and compare the result with the results of Ref. [10]. These studies are in progress.

ACKNOWLEDGMENTS

The authors thank T. Tanaka, K. Yamada, T. Narikawa, K. Nakashi, and K. Nakao for useful comments. This work was supported by JSPS KAKENHI Grants No. 18J10275 (K. O.), No. JP19K14715 (T. I.), No. JP19K03876 (T. H.), No. JP18K03652 (U. M.) and the MEXT-Supported Program for the Strategic Research Foundation at Private Universities (S1411024) (T. I., T. H.). K. O. is grateful to the Yukawa Institute for Theoretical Physics at Kyoto University, where this work was developed during "The 3rd Workshop on Gravity and Cosmology by Young Researchers" (YITP-W-18-15).

[1] K. Akiyama *et al.* (Event Horizon Telescope Collaboration), First M87 event horizon telescope results. I. The shadow of the supermassive black hole, Astrophys. J. **875**, L1 (2019).
[2] V. Cardoso and P. Pani, Testing the nature of dark compact objects: A status report, Living Rev. Relativity **22**, 4 (2019).
[3] R. Penrose, Gravitational collapse: The role of general relativity, Nuovo Cimento **1**, 252 (1969).
[4] T. Piran, J. Shaham, and J. Katz, High efficiency of the Penrose mechanism for particle collisions, Astrophys. J. **196**, L107 (1975).
[5] M. Banados, J. Silk, and S. M. West, Kerr Black Holes as Particle Accelerators to Arbitrarily High Energy, Phys. Rev. Lett. **103**, 111102 (2009).
[6] T. Harada and M. Kimura, Black holes as particle accelerators: A brief review, Classical Quantum Gravity **31**, 243001 (2014).
[7] J. D. Schnittman, Revised Upper Limit to Energy Extraction from a Kerr Black Hole, Phys. Rev. Lett. **113**, 261102 (2014).
[8] E. Berti, R. Brito, and V. Cardoso, Ultrahigh-Energy Debris from the Collisional Penrose Process, Phys. Rev. Lett. **114**, 251103 (2015).
[9] O. Semerak, Photon escape cones in the Kerr field, Helv. Phys. Acta **69**, 69 (1996).
[10] D. V. Gal'tsov and K. V. Kobialko, Completing characterization of photon orbits in Kerr and Kerr-Newman metrics, Phys. Rev. D **99**, 084043 (2019).
[11] S. Chandrasekhar, *The Mathematical Theory of Black Holes* (Oxford University Press, Oxford, 1998), p. 646.
[12] K. Ogasawara, T. Harada, U. Miyamoto, and T. Igata, Escape probability of the super-Penrose process, Phys. Rev. D **95**, 124019 (2017).
[13] B. Carter, Global structure of the Kerr family of gravitational fields, Phys. Rev. **174**, 1559 (1968).
[14] J. M. Bardeen, W. H. Press, and S. A. Teukolsky, Rotating black holes: Locally nonrotating frames, energy extraction, and scalar synchrotron radiation, Astrophys. J. **178**, 347 (1972).
[15] T. Igata, H. Ishihara, and Y. Yasunishi, Observability of spherical photon orbits in near-extremal Kerr black holes, Phys. Rev. D **100**, 044058 (2019).
[16] J. Feng and Q. Wu, Constraint on the black-hole spin of M87 from the accretion-jet model, Mon. Not. R. Astron. Soc. **470**, 612 (2017).